

Interface dynamics and crystal phase switching in GaAs nanowires

Daniel Jacobsson^{1,2}, Federico Panciera^{3,4}, Jerry Tersoff⁴, Mark C. Reuter⁴, Sebastian Lehmann¹, Stephan Hofmann³, Kimberly A. Dick^{1,2} & Frances M. Ross⁴

Controlled formation of non-equilibrium crystal structures is one of the most important challenges in crystal growth. Catalytically grown nanowires are ideal systems for studying the fundamental physics of phase selection, and could lead to new electronic applications based on the engineering of crystal phases. Here we image gallium arsenide (GaAs) nanowires during growth as they switch between phases as a result of varying growth conditions. We find clear differences between the growth dynamics of the phases, including differences in interface morphology, step flow and catalyst geometry. We explain these differences, and the phase selection, using a model that relates the catalyst volume, the contact angle at the trijunction (the point at which solid, liquid and vapour meet) and the nucleation site of each new layer of GaAs. This model allows us to predict the conditions under which each phase should be observed, and use these predictions to design GaAs heterostructures. These results could apply to phase selection in other nanowire systems.

Many materials can grow in multiple (meta)stable crystal structures, and phase selection is one of the most fundamental problems in materials science. However, the selection process is difficult to access experimentally; for example, many metastable phases are obtained only by rapid quenching of a liquid into a polycrystalline multiphase solid. By contrast, nanowires provide an ideal system for studying phase selection. Typical zinc-blende (ZB)-structure III-V semiconductors form nanowires in the wurtzite (WZ) structure as well as the ZB^{1–5}. Nanowires can easily be switched between these phases by varying the temperature, source-material flux or impurities^{3,4,6–14}, and their small diameter guarantees that they are single crystals, with phase switching occurring along the growth axis where it is easily observed. ZB and WZ semiconductors have different band structures¹⁵, which creates opportunities for designing modulated nanowire structures with new electronic properties. Crystal phase heterostructures are particularly interesting because they can access the electronic properties of heterostructure quantum dots for photonics and single-electron-transistor applications, but without the challenge of achieving compositional control^{16–19}.

To take full advantage of the possibilities offered by crystal structure control, a detailed understanding of the physics behind crystal phase selection is required. On the basis of post-growth observations, different models have been proposed for phase selection. These models emphasize the role of supersaturation, catalyst geometry and interfacial energies^{20–25}. Experimental results are typically interpreted in terms of the dominant role of one of these factors^{6–8,10,12,20,26–28}.

Here, we directly observe the dynamic processes that take place during nanowire growth for each crystal phase, and during the switch between phases, using *in situ* transmission electron microscopy. We find surprising differences in the structure and dynamics during growth of ZB and WZ nanowires. The switching process itself, and the associated changes in geometry, provide clues that allow us to develop a new model identifying the underlying mechanism driving crystal phase selection. In this model, droplet geometry is the key parameter in determining structure, but in an indirect way, via its effect on the nanowire edge morphology. This understanding allows us to form crystal phase quantum dots with atomic layer precision.

Imaging interface and catalyst geometry

We observed the two GaAs nanowire crystal phases during growth *in situ* using a Hitachi H-9000 ultra-high vacuum transmission electron microscope (UHVTEM)^{29,30}. Si substrates were first covered with pre-grown GaAs nanowires using standard metal-organic vapour phase epitaxy (MOVPE) and Au aerosol particles with diameters of 30 nm, 50 nm and 70 nm. Such samples were loaded into the TEM and heated resistively, using a pyrometer to calibrate the temperature at each heating current (see Methods). Pure trimethylgallium (TMGa) and arsine (AsH₃) were used as precursor gases, and were introduced close to the substrate using separate capillary tubes to a maximum total pressure during imaging of 2×10^{-5} Torr. Details of how the growth parameters *in situ* compare to conventional MOVPE are provided in Methods. On heating to temperatures of about 550 °C, a liquid AuGa droplet formed at the nanowire tips and growth took place at the droplet/nanowire interface. Growth was recorded at 30 images per second. Dark-field imaging conditions, as used in Fig. 1, allow the crystal structure to be distinguished, that is, the WZ phase and the two twin variants of the ZB phase (Extended Data Fig. 1). Bright-field imaging conditions, as used in Fig. 2, allow a more accurate determination of the dimensions of the droplet and the nanowire.

We find that, *in situ*, both ZB and WZ GaAs can be grown by varying the precursor pressures (the V/III ratio) while maintaining a constant temperature. Within the parameter range accessible *in situ*, WZ GaAs forms at higher V/III ratios and ZB at lower ratios at steady-state conditions; transient conditions are discussed below. The two phases show marked differences in terms of their growth dynamics. For WZ GaAs, growth proceeds by step flow across the droplet/nanowire interface (Fig. 1a and Supplementary Video 1). Steps flow slowly with each one starting as soon as the previous one has completed its flow (Extended Data Fig. 2a). By counting the number of step-flow events and correlating with the length of the nanowire (Extended Data Fig. 2b), as in ref. 31, we find that each step flow represents the addition of one WZ GaAs(0001) bilayer, with a height of 0.3 nm. The growth rates are low under the conditions accessible *in situ*, typically one bilayer per minute (see Methods and Supplementary Video 1). Growth rates are proportional to AsH₃ pressure (Extended Data Fig. 2c), which suggests

¹Solid State Physics and NanoLund, Lund University, Box 118, 221 00 Lund, Sweden. ²Centre for Analysis and Synthesis, Lund University, Box 124, 221 00 Lund, Sweden. ³Department of Engineering, University of Cambridge, 9 JJ Thomson Avenue, Cambridge CB3 0FA, UK. ⁴IBM T. J. Watson Research Center, 1101 Kitchawan Road, Yorktown Heights, New York 10598, USA.

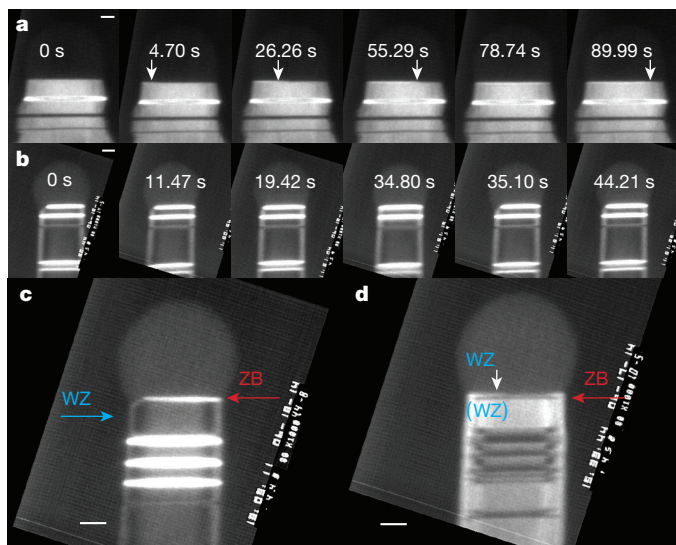


Figure 1 | Interface dynamics during WZ and ZB growth of GaAs.

a, Images extracted from a dark-field movie recorded during WZ GaAs growth. A step flows across the top facet of a nanowire that has a diameter of 60 nm; the position of the step is indicated by the arrows. See also Supplementary Video 1. Growth conditions: 550 °C, AsH₃ pressure of 1×10^{-5} Torr, TMGa pressure of 3.5×10^{-8} Torr. The narrow stripes show previously grown ZB segments: ZB can occur in two twinned orientations, one appearing bright and the other dark in this imaging condition. **b**, Images extracted from a dark-field movie recorded during ZB GaAs growth. The truncation slowly fills then jumps back to its maximum size (the simultaneous rapid step flow across the growth interface is not visible). See also Supplementary Video 2. Growth conditions (not steady-state for this example): 550 °C, AsH₃ pressure increased from 10^{-7} Torr to 1.4×10^{-5} Torr a few seconds before the first image was recorded, TMGa pressure of 2.0×10^{-8} Torr. ZB phases appear bright and WZ dark in this imaging condition. Note that the truncation shows strongly on one side of the nanowire; this was typical (see text), although some (5%) nanowires showed synchronized oscillation on both sides, as in Supplementary Video 5. The relative time of each image in **a** and **b** is shown in seconds. **c**, The first ZB bilayer growing on WZ, with imaging conditions as in **b**. The AsH₃ pressure was reduced; the droplet is in the process of growing larger past the critical volume; the first layer of ZB appears followed immediately by a truncation that cuts into the previously grown WZ. **d**, The first WZ bilayer growing on a ZB segment. The AsH₃ pressure was increased; the droplet is in the process of growing smaller; the truncation fills in and the first layer of WZ appears via step flow. The truncation does not appear, and slow step flow occurs, even though ZB covers the top facet. Scale bars are 10 nm in all images.

that growth under these circumstances is limited by the arrival and incorporation of As (see Methods). We can then understand the step-flow dynamics through the solubility of As in AuGa, which is generally accepted to be low³². Since the droplet contains no reservoir of the rate-limiting species (in our case, As), the arriving atoms are incorporated immediately into the nanowire, leading to slow and gradual step flow³³.

The growth of ZB GaAs looks quite different (Fig. 1b, Supplementary Video 2). Growth similarly proceeds by addition of bilayers, but each bilayer flows across the growth interface too rapidly to observe. Furthermore, the droplet/nanowire interface shows an oscillating geometry at the trijunction (at which solid, liquid and vapour meet) that is similar to that seen in Si, ZB GaP, Ge and Al₂O₃ (refs 30, 31, 34, 35). The edge of the nanowire appears truncated (Fig. 1b, first panel). The three-dimensional geometry of this ‘edge facet’ is shown schematically in Extended Data Fig. 1. Material gradually adds to the edge facet to fill in the corner (Fig. 1b, second and third panels). The interface jumps forwards as one step flows quickly, and the edge facet reappears (Fig. 1b, fourth and fifth panels).

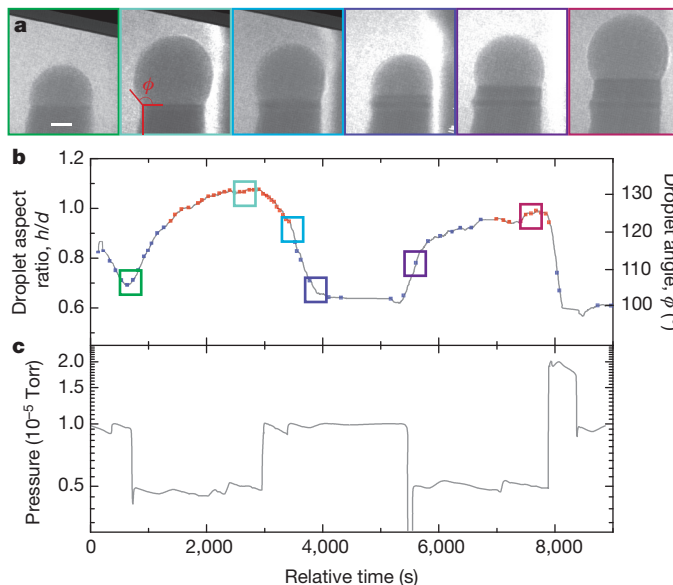


Figure 2 | Changes in droplet volume during phase switching. **a**, Series of bright-field images obtained during growth of a GaAs nanowire at varying AsH₃ pressure, constant TMGa pressure (2×10^{-8} Torr) and constant temperature (550 °C). Scale bar is 10 nm. **b**, Droplet aspect ratio h/d and angle ϕ as defined in **a**. The times of the images in **a** are indicated by coloured boxes. The droplet volume takes several minutes to respond to the change in pressure. The crystal phase is indicated by blue (WZ) and red (ZB) squares. Each red square marks the occurrence of a truncation of the top facet and nucleation of a ZB bilayer. Each blue square marks the identification of WZ growth via step flow. **c**, AsH₃ pressure variation over time.

Each oscillation in trijunction geometry is correlated with the nucleation and flow of a new bilayer, as in ref. 31. The step moves quickly, even with no reservoir of As, because it is supplied by material from the truncated volume. A rough estimate of the change in the truncated volume is consistent with it being the source of the one bilayer of growth.

In parallel with the observed changes in the interface dynamics, the droplet geometry also changes as we vary the V/III ratio to achieve growth of WZ and ZB GaAs. Figure 2 and Supplementary Video 3 show the effect on the droplet of changing the AsH₃ pressure between high values (to achieve WZ) and low values (to achieve ZB) at constant TMGa pressure (2×10^{-8} Torr). Temperature was kept constant throughout the experiments (at 540–560 °C) to avoid introducing temperature dependencies that would obscure the observed trends (see Methods). Throughout the changes in AsH₃ pressure, the nanowire continued to grow. The most obvious feature is the change in the volume of the droplet. We quantify this in Fig. 2b via the droplet aspect ratio h/d (droplet height divided by nanowire diameter at the growth interface) or, equivalently, via the droplet angle ϕ (angle between the basal plane and the tangent to the droplet at its edge; see Fig. 2a). On decreasing the AsH₃ pressure, the droplet increases in volume; increasing the AsH₃ pressure decreases the droplet volume. A quasi-steady-state volume is reached, depending on the V/III ratio. These volume changes must be driven by the addition or subtraction of Ga: we do not expect Au to move in and out of the droplet, because its diffusion on GaAs is assumed to be negligible at this temperature³⁶, whereas As makes up only a small fraction of the volume, owing to its low solubility (discussed above). An Au–Ga–As alloy with over 40% Ga forms a liquid at this temperature, with no upper limit on the Ga content³²; consequently, droplets of a range of volumes are possible. Furthermore, because the volume changes occur more quickly than the rate at which Ga could be consumed by incorporation into the growing nanowire, the Ga must be supplied or removed

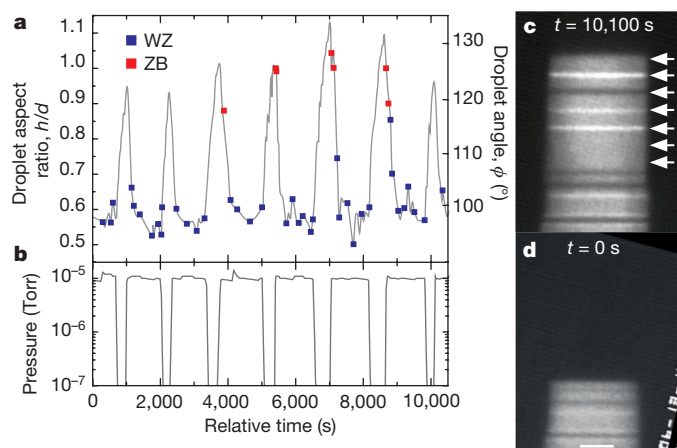


Figure 3 | Growth of a WZ nanowire containing multiple narrow ZB segments. TMGa pressure (2×10^{-8} Torr) and temperature (550°C) were constant. **a**, Droplet aspect ratio h/d and angle ϕ versus time (grey line), and crystal phase versus time (squares). Each square indicates the addition of a bilayer of WZ (blue) or ZB (red), as described in Fig. 1. ZB segments with thicknesses of zero, one or two bilayers form each time h/d increases. **b**, AsH_3 pressure variation over time. The pressure was held at 1×10^{-5} Torr to grow WZ, but was pulsed downwards to less than 10^{-8} Torr for seven intervals with durations 5 min, 5 min, 7 min, 7 min, 9 min, 9 min and 5 min, respectively. **c**, **d**, Images of the nanowire at the start (**d**) and end (**c**) of the experiment; scale bar is 10 nm. In **c**, the position of the growth front at each of the seven intervals is indicated by an arrow. The ZB segments grown in the 7- and 9-min intervals are visible as narrow stripes. Three segments have one ZB twin orientation (bright contrast in this imaging condition) and one has the other ZB twin orientation (dark contrast).

by surface diffusion along the nanowire. In the simplest picture³⁰, there is a surface reservoir of mobile Ga adatoms that equilibrate with the droplet over time whenever the chemical potentials of Ga in the droplet (and on the surface) are changed by altering the AsH_3 pressure. In this way, the V/III ratio controls the droplet size. (A more complete treatment would include diffusion and the effect of As flux on Ga diffusion, but this would not change the general picture²².)

We have shown above that crystal structure and droplet volume both change as the V/III ratio varies. We now explore how they correlate with each other. During a growth experiment, it is possible to measure crystal structure and droplet volume by alternating between dark- and bright-field imaging conditions. The crystal structure identified during the experiment in Fig. 2a is shown as the red and blue data points in Fig. 2b. It is clear that the switch between WZ and ZB crystal structure occurs as the droplet passes a certain aspect ratio—under these conditions, this is $h/d \approx 0.95$ and $\phi \approx 125^\circ$. (Other experiments show a small hysteresis that is not visible in this data; see, for example, Supplementary Fig. 3.) Because the droplet takes several minutes to respond to the pressure change, it is clear that WZ–ZB growth is correlated to h/d and ϕ rather than to the instantaneous AsH_3 pressure. This direct correlation between crystal switch and droplet dimensions (volume, aspect ratio and angle), governed ultimately by the V/III ratio, is a key result that provides the basis for the model we develop below.

Understanding that the droplet geometry is the critical parameter, rather than the gas environment itself, provides useful guidance in growing crystal phase heterostructures. The length of each crystal phase segment depends on the time during which the droplet has the appropriate geometry. The relatively slow kinetics of the change in droplet volume mean that the V/III ratio must be designed with appropriate offsets in timing. An example is shown in Fig. 3. Here, the V/III ratio was set initially at a value that formed WZ GaAs.

The AsH_3 pressure was then decreased, for short pulses, to a V/III ratio that would be expected to form ZB GaAs. The result is a series of ZB inclusions in a WZ nanowire with lengths that are repeatable, but not directly proportional to the pulse duration. The shortest pulses did not form ZB GaAs at all. Longer pulses produced one or two bilayers of ZB stacking. The correlation between droplet volume and crystal phase in Fig. 3 confirms that the droplet must reach a critical volume for the structural change to occur; the reduction of AsH_3 pressure in itself may not trigger a structure change. Designing a crystal phase heterostructure thus requires consideration of the kinetics of the change in droplet volume.

A model for interface geometry

Developing a framework to understand the relationship observed above between droplet volume, interface growth dynamics and crystal structure requires two additional key observations. The first observation is that when the droplet changes volume, it changes composition too. This could in principle affect phase selection, for example, by changing the surface energy²⁷. It is therefore not immediately clear which factor determines crystal structure, the Au:Ga ratio or the geometry (h/d and ϕ). To establish this we measured h/d and ϕ at the switch for one particular nanowire, then allowed the nanowire to increase its diameter by conformal growth on the sidewalls, and again measured h/d and ϕ while inducing a switch (Extended Data Fig. 3). Because the nanowire widens, but the amount of Au present does not change, relatively more Ga is needed to achieve the same h/d and ϕ . We did not see any strong effect of diameter on the switch between crystal phases; h/d and ϕ appear to be the controlling parameters.

The second observation concerns the relationship between crystal phase and the dynamics at the growth front. In Fig. 1c, d and Supplementary Videos 2 and 4 we show the crystal switch in more detail, specifically the growth of the first ZB layer on WZ GaAs and the first WZ layer on ZB GaAs. Starting from a WZ nanowire, we reduce the AsH_3 pressure (Fig. 3c); the droplet enlarges and the first ZB layer forms as the critical h/d and ϕ are reached. As the ZB step flows (too rapidly to see) across the growth interface, an edge facet appears (Supplementary Video 4). This facet cuts into the WZ beneath. Thus, even though steady-state growth of WZ GaAs proceeds without an edge facet, it is possible to form an edge facet in WZ GaAs under appropriate conditions. Conversely, if we start from a ZB nanowire and increase the AsH_3 pressure, as shown in Fig. 1d, then the droplet shrinks and the first WZ layer grows. It grows by slow step flow and without an edge facet appearing (Supplementary Video 2), even though ZB is exposed on the growth interface as it starts to grow.

These morphology observations are particularly surprising. One might expect the presence of an edge facet to be controlled by the crystal structure at that facet; but, instead, Fig. 1c, d shows that it correlates with the crystal structure on the main (that is, ZB(111) or WZ(0001)) growth facet, and thus with h/d and ϕ . To determine cause and effect, we analyse the ways in which the droplet angle ϕ affects the morphology of the growth interface. Equilibrium crystal shapes generally do not have edge angles as sharp as 90° , so one would expect an edge facet in a GaAs crystal. A sharp edge only exists during nanowire growth because the droplet is present, providing a capillary force that can pull on the edge facet and shrink its size to zero. We calculate the circumstances under which this occurs. We assume an ideal, symmetric nanowire for which the droplet angle ϕ is the same all around the edge (see Fig. 4a); the more realistic, asymmetric case is discussed below. The difference in free energy between this ideal nanowire with an edge facet and a nanowire with the same geometry but a sharp edge is³¹

$$\Delta E = c_1 y L + \frac{1}{2} y^2 (\cot \theta) (\mu_{\text{cat}} - \mu_0) L + c_2 y^2 L \quad (1)$$

in which L is the total length of the edge, y is the facet length and θ is the facet angle (see Fig. 4a), $\mu_{\text{cat}} - \mu_0$ reflects the supersaturation

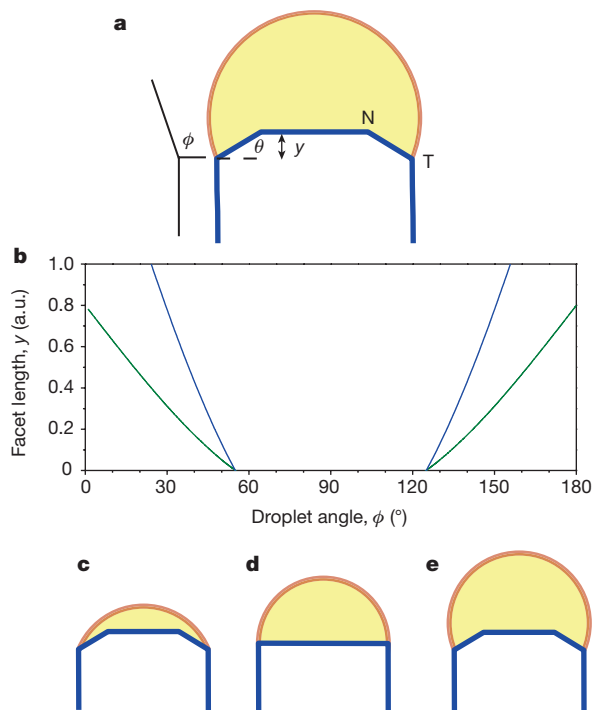


Figure 4 | Model relating droplet size to interface morphology. **a**, Schematic of a quasi-two-dimensional, ideal, symmetric nanowire illustrating the droplet angle ϕ , and the edge facet angle θ and length (in the growth direction) y . ‘N’ marks the interior point at which ZB nucleates; ‘T’ marks the trijunction. **b**, Edge facet length y versus droplet angle ϕ , calculated for two values of supersaturation (blue, low; green, high) for the symmetric nanowire. There is a range of ϕ in which $y=0$; in this range $c_1 > 0$ and the edge facet does not exist. Supersaturation does not affect this range. **c–e**, Schematics of the nanowire and droplet for $\phi < 90^\circ$ (**c**), $\phi = 90^\circ$ (**d**) and $\phi > 90^\circ$ (**e**). The possibility of the droplet depinning from the point T is not included in the model.

of chemical potential μ in the catalyst, and c_2 includes various other second-order terms³¹. For a sufficiently small facet length y , this energy is dominated by the linear term c_1 , which reflects the capillary forces acting on the corner facet. Therefore, for $c_1 < 0$, it is always energetically favourable to have the edge facet ($\Delta E < 0$), whereas for $c_1 > 0$, we expect the edge to be sharp everywhere and have no facet. By examining c_1 in more detail and including all the capillary terms³⁷, we find

$$c_1 = \gamma_e \frac{1}{\sin \theta} - \gamma_{vs} - \gamma_{ls} \frac{\cos \theta}{\sin \theta} + \gamma_{vl} \sin \phi \quad (2)$$

in which γ_e is the liquid–solid interfacial energy at the edge facet, γ_{vs} is the vapour–solid interfacial energy on the sidewall, γ_{ls} is the liquid–solid interfacial energy at the main growth facet and γ_{vl} is the vapour–liquid interfacial energy.

The key point here is the presence of ϕ in equation (2). This implies that the droplet angle alters c_1 and, hence, changes the lowest-energy state of the nanowire from one with an edge facet to one with a sharp corner. A hemispherical droplet ($\phi = 90^\circ$) yields the maximum possible value of c_1 , and so is the most favourable for eliminating the edge facet. This is shown in Fig. 4b, in which we calculate the length y of the edge facet as a function of angle ϕ for a symmetric, but otherwise arbitrary, illustrative case. In our experiments, the droplet is never less than a hemisphere (ϕ is always greater than 90°) during stable growth. Thus, the analysis in equations (1) and (2) predicts that a switch could be observed between a large droplet with an edge facet (Fig. 4e) and a smaller droplet with a sharp edge (Fig. 4d); that is indeed what we observe.

Connecting geometry to crystal phase

We now consider the ways in which the presence or absence of an edge facet controls the crystal phase. Without attempting to develop a microscopic model, we can understand heuristically how this would occur by considering a previous analysis²⁰. Several models have argued that the crystal structure should be determined by the location of the nucleation event on the main growth facet^{6–8,10,13,20–23,26,38}. The argument is that the metastable WZ phase can only grow if it has a lower nucleation barrier than does the ZB phase. With sharp edges, nucleation is expected to occur at the trijunction (rather than in the middle of the facet), so the solid–vapour interface plays a critical part. In particular, the solid–vapour interface energy is thought to be lower for WZ nanowires, reducing the nucleation barrier for WZ relative to ZB in this geometry²⁰. However, when edge facets are present, nucleation on the main facet occurs away from the trijunction (presumably at position ‘N’ in Fig. 4a; ref. 31) and the liquid–vapour interface plays no part. If we adopt this argument, then it is no surprise that the change in the trijunction geometry can result in easier nucleation of WZ than ZB in one case, but not the other. This argument is also qualitatively consistent with *in situ* X-ray diffraction studies that infer (indirectly) that crystal structure in GaAs nanowires is determined by the geometry of the liquid–vapour interface^{39,40}. Here, we have not considered effects of interlayer interactions on the nucleation barrier, which might lead to formation of higher-order crystal phases, such as 4H, under certain conditions⁴¹, because we do not observe such phases in our experiments.

At very small h/d , our analysis also suggests the possibility of an edge facet and, hence, ZB growth (Fig. 4b). Although we cannot access such conditions in our experiments, they could occur transiently at the beginning of nanowire growth, because the droplet has much a smaller h/d ratio when sitting on a flat surface⁴², and perhaps at the end of growth if material in the droplet is consumed. Indeed, the ZB phase has been observed at the bases and tips of WZ nanowires²⁰, although under growth conditions that are different enough that our model might not be applicable. Recent experiments have demonstrated two transitions (from ZB to WZ and then back to ZB) as the V/III ratio is increased⁹, consistent with the model in Fig. 4. However, because our experiments have only a limited range of V/III ratios, we cannot observe the second transition back to ZB and so cannot assess whether the transition is associated with interface structure in a way that is analogous to the switch at lower group V pressures.

The discussion above is simplified in several respects. No difference in interfacial or surface energies between ZB and WZ structures is included. The small, but real, differences could lead to hysteresis in the switching angle as the droplet grows and shrinks. However, data such as that in Fig. 2, which displays no strong hysteresis, suggest that the droplet angle has a larger effect than do the differences between ZB and WZ interfacial energies.

More importantly, our quasi-two-dimensional model treats the droplet angle ϕ as uniform all the way around the edge. For the true three-dimensional geometry, in which the droplet sits on a hexagonal prism whose side lengths may not be equal⁴³, it is clear that ϕ will vary around the trijunction. Suppose that for a WZ nanowire we change the conditions to enlarge the droplet. At some point, ϕ will become large enough along one edge for that edge to become truncated, even though other edges remain sharp. As the droplet continues to grow, every other edge will progressively become truncated. Therefore, we expect any nanowire with unequal edge lengths to exhibit a mix of sharp and truncated edges over a range of droplet volumes. In the experiments, we observe the ZB phase once the first truncated corner appears (Fig. 1 and Supplementary Videos 2 and 4). Because we typically stabilize the conditions as soon as we see the crystal switch, the majority of nanowires presented here show a mix of sharp and truncated edges. However, we also observe symmetrically oscillating nanowires (Supplementary Video 5), presumably because the wire is more symmetric or because the droplet has grown

large enough to cause all edges to be truncated. The observation mentioned above that the ZB phase grows if any edge is truncated, whereas WZ grows only when all edges are sharp, implies that nucleation of ZB at a truncated edge is actually easier than nucleation of either WZ or ZB at a sharp one. This somewhat unexpected result could provide guidance in refining model parameters in nucleation calculations.

Conclusions

Direct observation during growth has enabled us to probe the phenomena controlling crystal phase in nanowires. WZ and ZB crystal phases in GaAs appear markedly different during growth in terms of the morphology of the nanowire/droplet interface, the flow of steps and the droplet size. The step-flow kinetics can be understood as a consequence of As-limited growth, low As solubility in the droplet, and the role of the edge truncation as an alternative reservoir. Examining the switch between phases suggests a scenario in which the growth conditions (here, the V/III ratio) determine the volume of the droplet and, hence, its aspect ratio h/d and angle ϕ ; the value of ϕ determines whether an edge facet will be present; the presence or absence of the edge facet determines the nucleation site for a new layer; and the nucleation site determines which phase, WZ or ZB, is most likely to nucleate. Our interpretation differs markedly from previous models of phase selection. Because nanowire growth has been achieved using a wide range of parameters and growth techniques, it is possible that phase selection is controlled by different physics under different circumstances. However, the regime we analyse here, MOVPE under As-limited conditions, has advantages for atomic-level control and high-throughput manufacturing.

This understanding of the causal sequence, in particular the changes in droplet volume with conditions and the controlling role of the droplet angle ϕ , has practical consequences. First, the large changes in droplet volume as a function of conditions may be relevant to aspects of nanowire growth other than crystal phase control¹³. For example, kinking can be caused by depinning of droplets from the nanowire tip^{37,44}, and experiments such as those shown here can explore the range of conditions under which droplets attain sizes that are sufficiently large or sufficiently small to cause depinning. In terms of crystal phase control, because the Au:Ga ratio in the droplet seems not to be critical, our results might be applicable to self-catalysed (Au-free) nanowire growth (although any small difference in liquid surface energies could lead to a slightly different critical angle). A second consequence is that any means of controlling the energy balance between a truncated and sharp edge should affect the crystal phase: we used the V/III ratio here, but temperature and surfactants are other possible ways to tune the crystal phase. We anticipate that similar behaviour may occur in other III-V semiconductors that exhibit polytypism, although it is not guaranteed because the various interfacial-energy parameters are material-specific. Finally, understanding how crystal structure switching depends on the kinetics of group III motion into and out of the droplet helps us work towards precise control of individual crystal phase superlattices, to enable fabrication of new types of electronic devices that make full use of the possibilities for engineering band structure that are provided by crystal-phase-engineered nanowires.

Online Content Methods, along with any additional Extended Data display items and Source Data, are available in the online version of the paper; references unique to these sections appear only in the online paper.

Received 7 October 2015; accepted 6 January 2016.

1. Krogstrup, P. *et al.* Structural phase control in self-catalyzed growth of GaAs nanowires on silicon (111). *Nano Lett.* **10**, 4475–4482 (2010).
2. Ikejiri, K., Kitauchi, Y., Tomioka, K., Motohisa, J. & Fukui, T. Zinc blende and wurtzite crystal phase mixing and transition in indium phosphide nanowires. *Nano Lett.* **11**, 4314–4318 (2011).
3. Husanu, E., Ercolani, D., Gemmi, M. & Sorba, L. Growth of defect-free GaP nanowires. *Nanotechnology* **25**, 205601 (2014).

4. Caroff, P. *et al.* Controlled polytypic and twin-plane superlattices in III-V nanowires. *Nature Nanotechnol.* **4**, 50–55 (2009).
5. Koguchi, M., Kakibayashi, H., Yazawa, M., Hiruma, K. & Katsuyama, T. Crystal structure change of GaAs and InAs whiskers from zinc-blende to wurtzite type. *Jpn J. Appl. Phys.* **31**, 2061–2065 (1992).
6. Wallentin, J. *et al.* Changes in contact angle of seed particle correlated with increased zincblende formation in doped InP nanowires. *Nano Lett.* **10**, 4807–4812 (2010).
7. Lehmann, S., Wallentin, J., Jacobsson, D., Deppert, K. & Dick, K. A. A general approach for sharp crystal phase switching in InAs, GaAs, InP, and GaP nanowires using only group V flow. *Nano Lett.* **13**, 4099–4105 (2013).
8. Joyce, H. J., Wong-Leung, J., Gao, Q., Tan, H. H. & Jagadish, C. Phase perfection in zinc blende and wurtzite III-V nanowires using basic growth parameters. *Nano Lett.* **10**, 908–915 (2010).
9. Lehmann, S., Jacobsson, D. & Dick, K. A. Crystal phase control in GaAs nanowires: opposing trends in the Ga- and As-limited growth regimes. *Nanotechnology* **26**, 301001 (2015).
10. Algra, R. E. *et al.* The role of surface energies and chemical potential during nanowire growth. *Nano Lett.* **11**, 1259–1264 (2011).
11. Dheeraj, D. L. *et al.* Controlling crystal phases in GaAs nanowires grown by Au-assisted molecular beam epitaxy. *Nanotechnology* **24**, 015601 (2013).
12. Johansson, J. *et al.* Effects of growth conditions on the crystal structure of gold-seeded GaP nanowires. *J. Cryst. Growth* **310**, 5102–5105 (2008).
13. Yuan, X. *et al.* Tunable polarity in a III-V nanowire by droplet wetting and surface energy engineering. *Adv. Mater.* **27**, 6096–6103 (2015).
14. Xu, T. *et al.* Faceting, composition and crystal phase evolution in III-V antimonide nanowire heterostructures revealed by combining microscopy techniques. *Nanotechnology* **23**, 095702 (2012).
15. De, A. & Pryor, C. E. Predicted band structures of III-V semiconductors in the wurtzite phase. *Phys. Rev. B* **81**, 155210 (2010).
16. Akopian, N., Patriarche, G., Liu, L., Harmand, J. C. & Zwiller, V. Crystal phase quantum dots. *Nano Lett.* **10**, 1198–1201 (2010).
17. Vainorius, N. *et al.* Confinement in thickness-controlled GaAs polytype nanodots. *Nano Lett.* **15**, 2652–2656 (2015).
18. Assali, S. *et al.* Direct band gap wurtzite gallium phosphide nanowires. *Nano Lett.* **13**, 1559–1563 (2013).
19. Dick, K. A., Thelander, C., Samuelson, L. & Caroff, P. Crystal phase engineering in single InAs nanowires. *Nano Lett.* **10**, 3494–3499 (2010).
20. Glas, F., Harmand, J. C. & Patriarche, G. Why does wurtzite form in nanowires of III-V zinc blende semiconductors? *Phys. Rev. Lett.* **99**, 146101 (2007).
21. Dubrovskii, V. G., Sibirev, N. V., Harmand, J. C. & Glas, F. Growth kinetics and crystal structure of semiconductor nanowires. *Phys. Rev. B* **78**, 235301 (2008).
22. Dubrovskii, V. G. Influence of the group V element on the chemical potential and crystal structure of Au-catalyzed III-V nanowires. *Appl. Phys. Lett.* **104**, 053110 (2014).
23. Krogstrup, P. *et al.* Advances in the theory of III-V nanowire growth dynamics. *J. Phys. D* **46**, 313001 (2013).
24. Johansson, J. *et al.* Effects of supersaturation on the crystal structure of gold seeded III-V nanowires. *Cryst. Growth Des.* **9**, 766–773 (2009).
25. Krogstrup, P. *et al.* Impact of the liquid phase shape on the structure of III-V nanowires. *Phys. Rev. Lett.* **106**, 125505 (2011).
26. Munshi, A. M. *et al.* Crystal phase engineering in self-catalyzed GaAs and GaAs/GaAsSb nanowires grown on Si(111). *J. Cryst. Growth* **372**, 163–169 (2013).
27. Cirilin, G. E. *et al.* Self-catalyzed, pure zincblende GaAs nanowires grown on Si(111) by molecular beam epitaxy. *Phys. Rev. B* **82**, 035302 (2010).
28. Spirkoska, D. *et al.* Structural and optical properties of high quality zinc-blende/wurtzite GaAs nanowire heterostructures. *Phys. Rev. B* **80**, 245325 (2009).
29. Ross, F. M. Controlling nanowire structures through real time growth studies. *Rep. Prog. Phys.* **73**, 114501 (2010).
30. Chou, Y.-C. *et al.* Atomic-scale variability and control of III-V nanowire growth kinetics. *Science* **343**, 281–284 (2014).
31. Wen, C. Y. *et al.* Periodically changing morphology of the growth interface in Si, Ge, and GaP nanowires. *Phys. Rev. Lett.* **107**, 025503 (2011).
32. Prince, A. A., Raynor, G. V. & Evans, D. S. *Phase Diagrams of Ternary Gold Alloys* 123–132 (Institute of Metals, 1990).
33. Wen, C. Y., Reuter, M. C., Tersoff, J., Stach, E. A. & Ross, F. M. Structure, growth kinetics, and ledge flow during vapour–solid–solid growth of copper-catalyzed silicon nanowires. *Nano Lett.* **10**, 514–519 (2010).
34. Oh, S. H. *et al.* Oscillatory mass transport in vapor-liquid-solid growth of sapphire nanowires. *Science* **330**, 489–493 (2010).
35. Gamalski, A. D., Ducati, C. & Hofmann, S. Cyclic supersaturation and triple phase boundary dynamics in germanium nanowire growth. *J. Phys. Chem. C* **115**, 4413–4417 (2011).
36. Hilner, E. *et al.* Au wetting and nanoparticle stability on GaAs(111)B. *Appl. Phys. Lett.* **89**, 251912 (2006).
37. Schwarz, K. W. & Tersoff, J. Elementary processes in nanowire growth. *Nano Lett.* **11**, 316–320 (2011).
38. Yu, X. *et al.* Evidence for structural phase transitions induced by the triple phase line shift in self-catalyzed GaAs nanowires. *Nano Lett.* **12**, 5436–5442 (2012).
39. Krogstrup, P. *et al.* In-situ x-ray characterization of wurtzite formation in GaAs nanowires. *Appl. Phys. Lett.* **100**, 093103 (2012).
40. Takahashi, M., Kozu, M., Sasaki, T. & Hu, W. Mechanisms determining the structure of gold-catalyzed GaAs nanowires studied by in situ X-ray diffraction. *Cryst. Growth Des.* **15**, 4979–4985 (2015).

41. Johansson, J., Zanolli, Z. & Dick, K. A. Polytype attainability in III–V semiconductor nanowires. *Cryst. Growth Des.* **16**, 371–379 (2016).
42. Schmidt, V., Senz, S. & Gösele, U. The shape of epitaxially grown silicon nanowires and the influence of line tension. *Appl. Phys. A* **80**, 445–450 (2005).
43. Jiang, N. *et al.* Understanding the true shape of Au-catalyzed GaAs nanowires. *Nano Lett.* **14**, 5865–5872 (2014).
44. Hillerich, K. *et al.* Strategies to control morphology in hybrid group III–V/group IV heterostructure nanowires. *Nano Lett.* **13**, 903–908 (2013).

Supplementary Information is available in the online version of the paper.

Acknowledgements D.J., S.L. and K.A.D. acknowledge financial support from the Knut and Alice Wallenberg Foundation (KAW), the Swedish Research Council

(VR) and the Nanometer Structure Consortium at Lund University (nmC@LU). F.P. and S.H. acknowledge support from ERC Grant 279342: InSituNANO. We acknowledge A. Ellis for technical support.

Author Contributions D.J. and F.P. performed experiments and data analysis, J.T. developed the model, M.C.R. developed the UHVTEM technique, S.L. provided growth expertise, and K.A.D., S.H. and F.M.R. designed the experiments and coordinated the analysis.

Author Information Reprints and permissions information is available at www.nature.com/reprints. The authors declare no competing financial interests. Readers are welcome to comment on the online version of the paper. Correspondence and requests for materials should be addressed to D.J. (Daniel.jacobsson@ftf.lth.se) or F.M.R. (fmross@us.ibm.com).

METHODS

The GaAs nanowires imaged in this study were grown on Si(111). The substrates were cut from a Si(111) wafer into strips $3\text{ mm} \times 350\text{ }\mu\text{m} \times 500\text{ }\mu\text{m}$, small enough to fit directly into the TEM heating holder. The strips were, however, too small to be handled in the GaAs growth system, so they were stacked in arrays, parallel to each other with the polished surface facing upwards, and mounted on a larger Si wafer. At Lund University, Au aerosol particles with diameters of 30 nm, 50 nm and 70 nm were deposited onto the arrays of strips using a size-selected aerosol source at a total density of about 1 particle per μm^2 . Then, GaAs nanowires of the order of 500 nm in length were grown on the arrays using standard metal–organic vapour phase epitaxy in an Epiquip system, operating at 100 mbar with AsH_3 and TMGa as precursor gases and H_2 as carrier gas. After growth, the arrays were glued to sample boxes using a small piece of SEM-type double-sided carbon tape, the sample boxes were placed in a plastic bag, which was vacuum sealed, and then the bag was sent through air to the UHVTEM at IBM. The individual strips were separated and each sample was degassed in UHV by resistive heating below $100\text{ }^\circ\text{C}$ for 30 min, flowing a direct current through the Si strip. The heating current required for a temperature of around $300\text{ }^\circ\text{C}$ was then determined in a separate UHV chamber using an infrared pyrometer. All of the strips had a similar temperature–current calibration, so it was possible to estimate the current required to heat the sample to $500\text{ }^\circ\text{C}$ or $550\text{ }^\circ\text{C}$. The sample was transferred to the UHVTEM column to check that the nanowires and Au catalysts were still present after this process. Finally, TMGa was flowed to a chosen pressure of around 5×10^{-8} Torr as measured using a mass spectrometer, AsH_3 was flowed to a chosen pressure of around 2×10^{-5} Torr as measured on the column ion gauge, the nanowires were heated to $500\text{--}550\text{ }^\circ\text{C}$ and GaAs was grown at the nanowire tips. The crystal phase was generally controlled using AsH_3 pressure, which was easier to measure and faster to change than TMGa. After experiments on one sample were completed, the full current–temperature calibration curve was obtained for that sample. The reason for this calibration procedure was to prevent any damage (for example, etching) of the wires by overheating before the growth experiment began. Owing to drift of the temperature on continued heating, we estimate the temperature accuracy to be $\pm 20\text{ }^\circ\text{C}$. All observations of crystal switching occurred between $500\text{ }^\circ\text{C}$ and $570\text{ }^\circ\text{C}$. Approaching $500\text{ }^\circ\text{C}$, the temperature range over which switching occurred became narrower and ZB grew for all accessible pressures. Above $600\text{ }^\circ\text{C}$, the nanowires etched slowly at the Au/GaAs interface, presumably owing to the low group V pressure.

This growth *in situ* within the TEM is somewhat different from standard MOVPE. Even though the conventional MOVPE precursor gases are used, there is no H_2 carrier gas during growth within the TEM, as is typically used during MOVPE growth of GaAs. In addition, the absolute pressures of the two precursor species are lower than typical precursor partial pressures used in MOVPE. The lower partial pressures can alone account for the low growth rates observed here compared to those observed in MOVPE. To compare the effects of the V/III ratio, we need to consider the possible differences between the two methods in more detail.

The growth in this study was observed to always be group-V limited, as seen in Extended Data Fig. 2c. This is in contrast to standard MOVPE, where high group-V flows and group-III-limited regimes are typically used. Instead, one could argue that the *in situ* TEM conditions are more similar or relevant to chemical beam

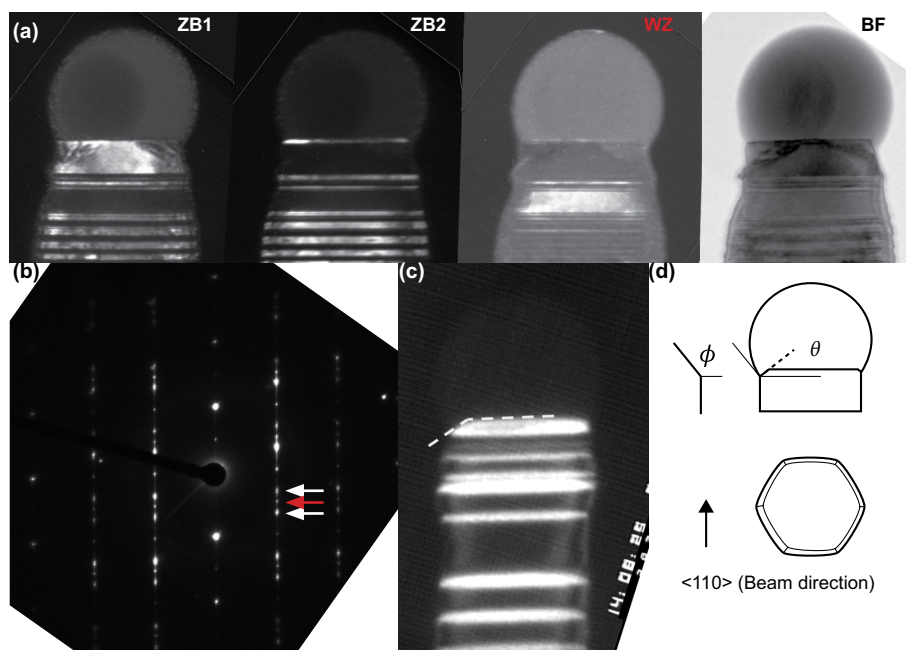
epitaxy (CBE), or possibly molecular beam epitaxy (MBE), than to MOVPE. The group-V-limited regime is also highly relevant to catalyst-free growth from Ga droplets. One exception for MOVPE is a recent study⁹ exploring group-V-limited regimes in a standard MOVPE reactor to grow WZ and ZB GaAs. In this work, it was shown that at low enough group-V flow to yield group-V-limited growth, WZ grows at 'high' V/III ratio, whereas ZB grows when the V/III ratio is lowered. This result is in contrast to the more well-known behaviour in the group-III-limited regime, in which ZB forms at high V/III ratio; however, the result of ref. 9 is entirely in agreement with the results of this study. Where the present work and that presented in ref. 9 differ is in the absolute magnitude of the V/III ratio: here, V/III ratios of 100 or more yielded group-V-limited nanowire growth; in ref. 9, the group-V-limited regime occurred at V/III ratios of less than 2.

This comparison suggests that the effective As pressure at the growth front is substantially lower in the TEM, relative to the Ga pressure, than in typical MOVPE. To understand this, we note that AsH_3 pyrolysis in GaAs growth is generally considered to proceed heterogeneously on GaAs surfaces, without interaction with the carrier gas⁴⁵. This pyrolysis starts with adsorption of AsH_3 onto the surface, followed by sequential dissociation of H atoms one by one, eventually leaving atomic As adsorbed on the surface⁴⁶. When AsH_3 is combined with TMGa, however, the two species decompose together, simultaneously, via adduct formation on the surface; this decomposition pathway does not involve hydrogen and is more efficient than the decomposition of either species alone⁴⁵. That the species decompose primarily on the surface is an important clue to the relatively inefficient supply of As in the UHVTEM. First, the nanowires are grown on Si substrates rather than on GaAs; although there is also ample GaAs surface on the pre-grown nanowire stubs, this surface is clearly different from the typical GaAs substrates used for MOVPE nanowire growth. Second, the surfaces are likely to be passivated with hydrogen when growth occurs in a H_2 atmosphere; the absence of H_2 here could affect the supply in a number of ways, changing, for example, the decomposition process and precursor surface diffusion. Finally, the decomposition process relies on the desorption of gas-phase As species. This adsorption process naturally depends on the partial pressure; because As has a substantially higher vapour pressure than Ga, the adsorption process of As will be reduced to a greater extent by the lower partial pressure.

Other minor differences between growth in the TEM and growth in a reactor are expected, owing to the experimental set-up. When using needle valves rather than standard mass-flow controllers to control the precursor flows, the experimental parameters are less accurately controlled than they are in dedicated epitaxy growth systems. At the high V/III ratios used ($\text{V/III} > 100$), the TMGa partial pressure is much lower than that of AsH_3 . A gauge reading the total pressure close to the sample is used to monitor the AsH_3 flow and provide fast feedback on the AsH_3 pressure at the sample. To monitor TMGa pressure, a mass spectrometer is used, with a controlled, steady pressure of TMGa set at the start of the experiment and generally held constant. The mass spectrometer is continuously used during the experiments to monitor any drift in the TMGa pressure.

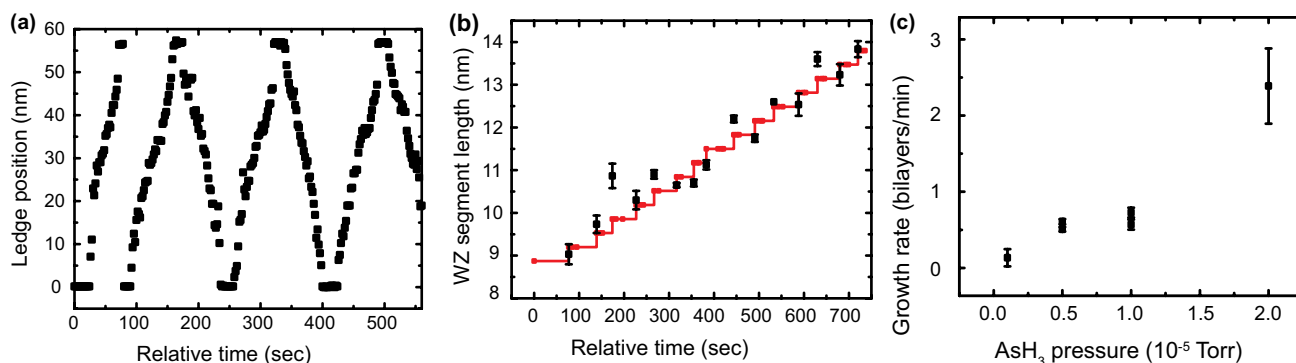
45. Larsen, C. A., Buchan, N. I. & Stringfellow, G. B. Reaction mechanisms in the organometallic vapor phase epitaxial growth of GaAs. *Appl. Phys. Lett.* **52**, 480–482 (1988).

46. Tamaru, K. The decomposition of arsine. *J. Phys. Chem.* **59**, 777–780 (1955).



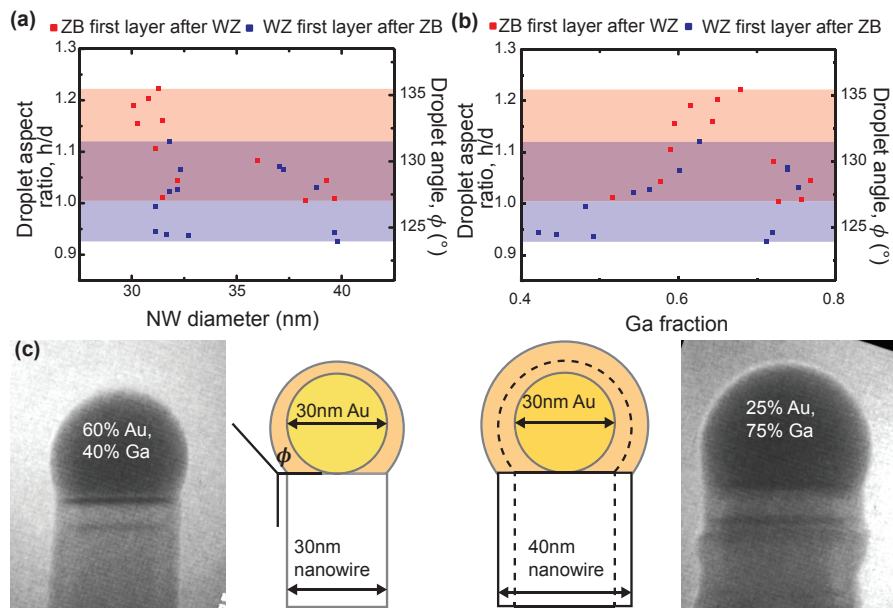
Extended Data Figure 1 | Distinguishing crystal phases using dark-field imaging. **a**, Dark-field images recorded using three spots in the diffraction pattern showing how WZ and the two variants of ZB (ZB1 and ZB2) are distinguished in the $\langle 110 \rangle$ direction. The right panel shows a bright-field (BF) image for comparison. **b**, Diffraction pattern with the three spots indicated. These are post-growth images recorded in a JEOL 3000 TEM.

c, Image recorded during growth, also in the $\langle 110 \rangle$ direction, showing the dark-field contrast and the measured angle of the truncated corner. **d**, A schematic showing the hexagonal cross-section as seen from the side (beam direction) and from above. Seen from the side, the droplet contact angle ϕ and corner-facet angle θ are shown. Seen from above, the electron beam direction is shown.



Extended Data Figure 2 | Kinetics of WZ growth. **a**, Step-flow kinetics measured for the WZ nanowire shown in Supplementary Video 1 and Fig. 1a. **b**, Length of a WZ nanowire versus the number of step-flow events. The average gradient of the graph confirms that each step is 0.33 nm in height, that is, a WZ(0001) bilayer. The red line shows the calculated length, assuming that each new bilayer (red squares) adds 0.33 nm in length. The black data are measured lengths, with error bars defined by

the standard deviation of each subset (length measured in 3–4 different movie frames for each data point). **c**, Growth rate versus AsH₃ pressure, estimated by measuring the increase in the length of the nanowire shown in Fig. 2 during growth intervals at different AsH₃ pressures, and by fitting a linear function to the length versus time plot. Error bars are defined by the standard error of the fits. The growth temperature was 550 °C and TMGa pressure was constant at 3.5×10^{-8} Torr.



Extended Data Figure 3 | Droplet angle at the transition does not change with Au composition in the droplet. a–c, During growth, the crystal structure of a nanowire was switched back and forth several times by changing the AsH_3 pressure. Data shows the measured angles and absolute droplet volumes at which the switch from WZ to ZB (red) and ZB to WZ (blue) occurred (a, b). During this time the wire also grew radially (c). a, Switch angles versus nanowire diameter. Shading indicates the range of observed angles at which WZ switches to ZB (red) and ZB to WZ (blue). Some hysteresis in switching is visible, perhaps because the droplet angle continues to change in the time before the switched layer grows. The data are scattered, but there is no strong dependence of angle on diameter (especially for the blue data points). For example, ZB switches to WZ at

angles between 123° and 132° at both large and small diameter, and WZ switches to ZB at angles between 127° and 136° . b, Switch angle versus inferred composition, as calculated from the measured h/d ratio assuming that the amount of Au does not change. The data are scattered, but there is no strong dependence of angle on composition. For example, for the first few data points, for which the nanowire had a diameter of 30 nm, ZB switched to WZ for a Ga fraction of less than 60%. For subsequent data points, for which the nanowire had a diameter of 40 nm, the switch did not occur until the composition had a Ga fraction of about 75%. The fact that droplet angles are similar despite the change in diameter suggests that droplet geometry controls the switch, whereas droplet volume and composition do not appear to be important.